American Mineralogist, Volume 74, pages 160–176, 1989

Order-disorder transition–induced twin domains and magnetic properties in ilmenite-hematite

GORDON L. NORD, JR., CHARLES A. LAWSON
959 National Center, U.S. Geological Survey, Reston, Virginia 22092, U.S.A.

ABSTRACT

The transition temperature (T_c) between disordered, $R\bar{3}c$, and ordered, $R\bar{3}$, ilmenite-hematite solid solutions in the ferrian ilmenite composition range between Ilm_{60} and Ilm_{80} has been redetermined by observing the presence or absence of transition-induced cation-ordered domains and the behavior of pre-existing domains annealed below the transition. The transition was reversed for Ilm_{70} and is bracketed between 1000 and 1050 °C. The domains were shown by dark-field transmission electron microscopy to be twin related by a 180° rotation about an axis parallel to **a** and to vary in size depending on T_c and the temperature of quench.

A model of the twin-domain boundary indicates that such boundaries are disordered and partially Fe-enriched. Magnetic and TEM observations on the same samples show that the room-temperature saturation magnetization is related to the surface area of the twin boundaries. Because the cation-ordered domains are ferrimagnetic with a strong magnetic moment and the disordered boundaries are probably antiferromagnetic with a weak magnetic moment, the quenched samples are essentially mixtures of two magnetic phases. The magnetization is therefore related to the proportion of each phase.

The twin boundaries act as the classic "x" phase, which allows ferrian ilmenite to acquire a self-reversed thermoremanent magnetization (TRM). Our measurements indicate that when the surface area of the twin boundaries in Ilm_{70} exceeds approximately 25×10^6 m^2/m^3, the quenched samples acquire reverse TRM during cooling in a 0.5-Oe field. When the boundary surface area is less than this critical threshold, the quenched samples acquire a normal TRM.

INTRODUCTION

Minerals of the ilmenite ($FeTiO_3$)–hematite (Fe_2O_3) solid-solution series have widespread importance in petrology and paleomagnetism. In petrology they provide, in conjunction with other coexisting Fe-bearing phases, information on oxygen fugacity, crystallization temperature, and cooling rates. In paleomagnetism they can make a substantial contribution to the magnetic signal of rocks. In particular, ferrian ilmenites in the composition range Ilm_{50} to Ilm_{75}, which are common in silicic volcanic rocks, can have a magnetic intensity approaching one-third that of magnetite.

The physical and chemical properties of natural and synthetic ilmenite-hematite solid solutions result in part from coupled interactions between cation order-disorder of Fe and Ti, phase separation in a miscibility gap, and magnetic order-disorder. These reaction boundaries are shown schematically in Figure 1. The locations of the reaction boundaries are not well known in the ilmenite-hematite binary because of difficulty in synthesis and characterization of the pure phase as well as slow reaction rates at the temperatures at and below those of the miscibility gap. The first and only experimental determination of the cation order-disorder transition curve was done by Ishikawa (1958) for compositions between $Ilm_{46.5}$ and Ilm_{68}. He found that the quenched, high-temperature, disordered phase is only weakly ferrimagnetic, whereas the quenched, low-temperature, ordered phase is strongly ferrimagnetic. In a series of annealing experiments, the point at which the room-temperature magnetization intensity changed was correlated by Ishikawa with the Fe-Ti cation order-disorder transition. Recent experimental and theoretical work on the phase-boundary topology suggests that the cation order-disorder transition is second-order in nature and intersects the top of the miscibility gap at a tricritical point near $Hem_{50}Ilm_{50}$ and 700 °C (Burton, 1984). As a consequence of the tricritical point, samples crystallizing on either side will experience very different phase transitions upon cooling (Allen and Cahn, 1976). Samples crystallizing in the $R\bar{3}c$ field with compositions more ilmenite-rich than Ilm_{50} will undergo cation ordering prior to exsolution upon cooling, whereas samples crystallizing in the $R\bar{3}c$ field with compositions less ilmenite-rich than Ilm_{50} will undergo clustering (exsolution); only the ilmenite-rich precipitate will order. The magnetic ordering transition (Fig. 1) decreases with increasing dilution by Ti until it is below room temperature at ilmenite-rich mole fractions.

0003–004X/89/0102–0160$02.00

The magnetic behavior of ilmenite-hematite solid solutions is unusual because samples in two compositional ranges (Ilm_{15-25} and Ilm_{51-73}) are capable of acquiring a reverse thermoremanent magnetization (reverse TRM). A "self-reversal" occurs when the remanent magnetization, which is acquired by a magnetic mineral when cooled through its Curie point in a magnetic field, is antiparallel to (or the reverse of) the applied field. In the first compositional range (Ilm_{15-25}) ilmenite-hematite solid solutions that have cooled very slowly in plutonic and metamorphic rocks can acquire a reverse TRM (Carmichael, 1961; Merrill and Gromme, 1967). The presence of the broad, two-phase miscibility gap results in the formation of exsolution microstructures in the rhombohedral oxides of these rocks. Slow cooling appears to be a necessary condition because only the titano-hematite portion (Ilm_{15} to Ilm_{25}) of exsolved grains carries the reversed remanence. Study of the self-reversal mechanism in this compositional range has been hampered by the nonreproducible nature of the reverse TRM in laboratory experiments. The cause of this type of reverse TRM is unknown but is thought to involve a magnetic coupling between two intimately intergrown phases.

The second compositional range is that of ferrian ilmenite, Ilm_{51-73}, where the limits were defined by Westcott-Lewis and Parry (1971b). Under certain crystallization and cooling conditions, ferrian ilmenite can acquire a reverse TRM. This type of self-reversal has been related directly to ferrian ilmenites that have undergone Fe-Ti ordering at high temperatures during cooling. Uyeda (1958) proposed a model for this self-reversal that required the interaction of a second magnetic phase with the host ferrian ilmenite. This second phase must (1) have a higher Curie temperature than the major phase (i.e., Fe-enriched), (2) have a disordered Fe-Ti distribution (i.e., antiferromagnetic), (3) be metastable with respect to annealing, and (4) couple antiferromagnetically with the host phase. This phase was called the "x" phase by Ishikawa and Syono (1963). The mechanism proceeds as follows. During cooling in a magnetic field, the high–Curie point "x" phase takes on the direction of the applied field. Upon further cooling, the lower–Curie point phase becomes magnetized in a direction antiparallel to the "x" phase (and thus, the applied field) because of a negative exchange interaction between it and the "x" phase. In nature, ilmenite-hematite minerals in this composition range are only found in acid extrusives and highly oxidized intermediate and basic extrusives.

Lawson et al. (1981) and Lawson and Nord (1984), using transmission electron microscopy, showed that synthetic ferrian ilmenite (Ilm_{70} and Ilm_{80}) grown at 1300 °C in the high-temperature, $R\bar{3}c$, disordered field (Fig. 1) forms transition-induced domains and domain boundaries upon cooling through the transition temperature into the low-temperature, $R\bar{3}$, ordered field. We also demonstrated that a high domain-boundary surface area was necessary for the operation of the magnetic self-reversal mechanism in synthetic Ilm_{70} and inferred that the domain boundary was the "x"-phase (Hoffman, 1975b, had previously suggested that antiphase boundaries could act as the "x" phase). Similarly, studies of dacitic pumice blocks from Mount Shasta, California, that exhibited reverse TRM showed the presence of a high density of transition-induced domain boundaries in ferrian ilmenite, Ilm_{58-59} (Lawson et al., 1987). This suggests that the same mechanism responsible for self-reversal in ferrian ilmenite synthesized in laboratory experiments is also responsible for self-reversal in natural ferrian ilmenites in dacitic volcanic rocks.

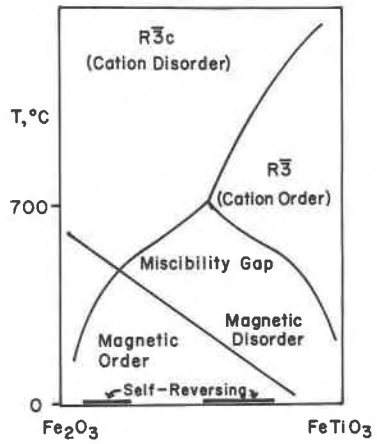

Fig. 1. Schematic ilmenite-hematite binary phase diagram showing the $R\bar{3}c$ to $R\bar{3}$ cation order-disorder transition, the miscibility gap between disordered hematite and ordered ilmenite and the magnetic order-disorder transition (Curie points). The cation order-disorder transition and miscibility gap intersect at a tricritical point at approximately 700 °C and Ilm_{50} (Burton, 1984). The two compositional fields of samples that exhibit a self-reversing thermoremanent magnetization are shown as heavy lines.

The goal of our research in the ilmenite-hematite binary is to map out the reaction boundaries and understand the changes in magnetic properties with time and cooling history. In this paper we are concerned only with the order-disorder transition in the composition range Ilm_{60} to Ilm_{100} and the magnetic properties of quenched Ilm_{70} samples. The location of the transition was determined by observing changes in domain microstructure that arise when samples are quenched from different temperatures above and below the transition. The kinetics of growth of the domains was monitored using samples that were heat-treated at different temperatures below the transition for different lengths of time. The result is an interpretation of the magnetic properties of ferrian ilmenite that considers the mechanism of formation and coarsening of the transition-induced microstructure, the kinetics of the high-temperature cation order-disorder transition, and the coupled interaction with the low-temperature magnetic ordering transition. It is the interaction between the microstructure and the magnetic transition that gives rise to the self-reversed TRM. The reader should note that the term "domain" in this paper will always

Table 1. Compositions and volumes of synthetic ilmenite-hematite

	900 °C		1300 °C				
	Ilm_{60}	Ilm_{70}	Ilm_{65}	Ilm_{70}	Ilm_{80}	Ilm_{90}	Ilm_{100}
TiO_2	30.9	36.3	33.76	36.01	41.99	47.03	52.65
FeO	27.9	32.6	30.34	32.41	37.71	42.26	47.36
Fe_2O_3	40.2	29.8	36.37	31.11	21.38	10.46	0.60
Total	99.0	98.7	100.47	99.53	101.08	99.75	100.61
Ilm (mol%)	60.6	70.9	64.96	69.84	79.72	90.00	99.43
No. analyses	14	13	14	13	14	10	12
(1σ)	(0.7)	(1.2)	(0.81)	(1.8)	(1.02)	(0.46)	(0.43)
V_{rh} (Å)	—	—	103.17	103.34	103.94	104.43	105.09
V_{hex} (Å)	—	—	309.51	310.02	311.82	313.29	315.27

* Oxides and totals are given after recalculation of ZAF-corrected microprobe data following Carmichael (1967).

refer to cation-ordered domains and not to magnetically ordered domains.

Experimental techniques

Compositions along the join Fe_2O_3-$FeTiO_3$ were synthesized at 1300 and 900 °C. Different experimental techniques were used for each temperature. Synthesis at 1300 °C was carried out by suspending sintered pellets of a Fe_2O_3 + TiO_2 mix in a vertical tube furnace through which flowed a mixture of CO_2-CO or CO_2-H_2 gas to control the oxygen fugacity. For a given composition, the oxygen fugacity in preliminary experiments was varied just until no magnetite-ulvöspinel phase was detected by light optical and SEM techniques in the run product. All of the 1300 °C Ilm_{70} runs were carried out in a vertical tube furnace fitted with a Y-doped zirconia cell at a $\log f_{O_2}$ of -5.68. After a synthesis time of 36 to 48 h, the pellets were dropped through the furnace into Hg or liquid N_2, resulting in a quench time to room temperature of approximately 10 s. Grain sizes produced by the gas-flow method at 1300 °C ranged from 30 to 80 μm. Synthesis at 900 °C was carried out using a stoichiometric mixture of TiO_2, Fe_2O_3, and Fe metal wrapped in Ag foil, which was then sealed in an evacuated silica-glass tube and heated for approximately two weeks. The silica-glass tube was dropped into water at the end of the experiment, resulting in a sample quench time to room temperature of approximately 1 min. Grain sizes in the 900 °C silica-glass tube samples averaged 5 μm. The silica-glass syntheses produced <5% magnetite-ulvöspinel in addition to the rhombohedral phase. A detailed discussion of the silica-glass tube synthesis can be found in Lawson (1978) and the gas-flow furnace synthesis in Lawson (1981) and Huebner (1987). Ilm_{70} pellets, synthesized at 1300 °C, were wrapped in Ag foil and annealed at 700–1000 °C in evacuated silica-glass tubes.

Run products were analyzed using reflected-light microscopy, electron-microprobe analysis, and X-ray powder diffraction (Table 1). Electron-microprobe analyses were conducted at the Geophysical Laboratory, Washington, D.C., using a MAC 400[1] electron microprobe operating at 15 keV. Matrix effects were corrected with the ZAF scheme of MAGIC IV. Fe_2O_3 was determined using the recalculation scheme of Carmichael (1967). Unit-cell volumes were calculated with a least-squares refinement program from Debye-Scherrer powder data using CaF_2 as an internal standard and Fe-filtered Co$K\alpha_1$ radiation.

[1] Use of brand names is for the purpose of identification only and does not constitute endorsements by the U.S. Geological Survey.

Transmission electron microscopy was conducted on a JEOL 200B operating at 200 keV at the U.S. Geological Survey, Reston, Virginia, and a Philips 420T operating at 120 keV at Johns Hopkins University, Baltimore, Maryland. Samples were first prepared as ultra-thin thin sections mounted with an acetone-soluble thermoplastic cement (see Wandless and Nord, 1986, for a description of this technique). Because of their fine-grained nature, the required final thicknesses achieved by hand polishing were often less than 10–15 μm. Portions of these were attached with superglue to either Cu grids or washers depending on the sample size and coherency and thinned to electron transparency by Ar-ion milling using 6-keV accelerating voltage and 18° tilt. A thin surface phase forms at 6-keV thinning voltages and is visible only as weak diffuse reflections in selected-area diffraction patterns. This phase was removed by final thinning at 1 keV for 24 h.

All diffraction patterns and real space planes and directions are indexed in the structural hexagonal unit cell by using the obverse setting of the hexagonal cell with respect to the rhombohedral cell. Although this statement may seem trivial, there is much confusion in the literature, especially in the indexing of hexagonal forms and planes (see Snow and Heuer, 1973).

The average domain size was measured by determining the average intercept length ($\bar{L}$) of a test line (L_T), following the technique of Smith and Guttman (1953). In this case, a standard test circle of approximately 10- or 15-cm circumference (L_T) was laid over the micrograph, and the number of circle-domain boundary intersections (N) counted. The circle was applied several times to each micrograph until greater than 50 intersections were counted. The average intercept length is then determined from the following relationship, where A is the number of applications of the test circle and M the magnification of the electron micrograph. The average domain size $\bar{L} = L_T(A)/N(M)$.

Smith and Guttman (1953) also pointed out that the average number of intercepts per unit length of a random line (test circle) drawn through a three-dimensional structure is exactly half the true ratio of surface to volume. Therefore, surface area per unit volume (S_V) was determined by the relationship $S_V = 2(N)(M)/L_T(A)$.

Saturation magnetization, J_s, was determined on an automated Curie balance at the Rock Magnetics Laboratory, Princeton University. Measurements were made at room temperature in fields up to a maximum of 7500 Oe. J_s was calculated by extrapolating the data to infinite field. The balance was calibrated with standard Ni samples. To check whether the reverse NRM of the samples is reproducible, we performed TRM acquisition experiments on the samples. For these experiments, the samples

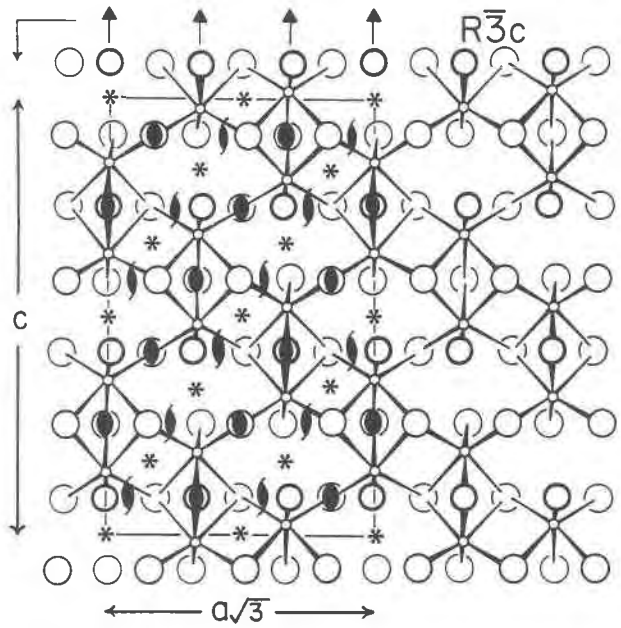

Fig. 2. Structure of $R\bar{3}c$ ilmenite-hematite projected on to $(11\bar{2}0)$. The **a** axis is normal to this view. Fe and Ti are disordered over the octahedral cation sites (small open circles) that lie in the plane of the diagram. The large heavy and light open circles represent oxygen atoms lying in front of and behind this plane, respectively. Groups of three oxygens called triplets form the common face of two face-sharing octahedra. In the $R\bar{3}c$ structure, these cation sites are equivalent, as in the corundum and hematite structure and the disordered hematite-ilmenite solid solutions. A twofold rotation axis pierces the triplet and relates the common cations. Other symmetry elements in the projection are shown: centers (shown as asterisks), twofold rotation and screw axes parallel to **a**, and **c**-glide and threefold rotation axes parallel to **c**.

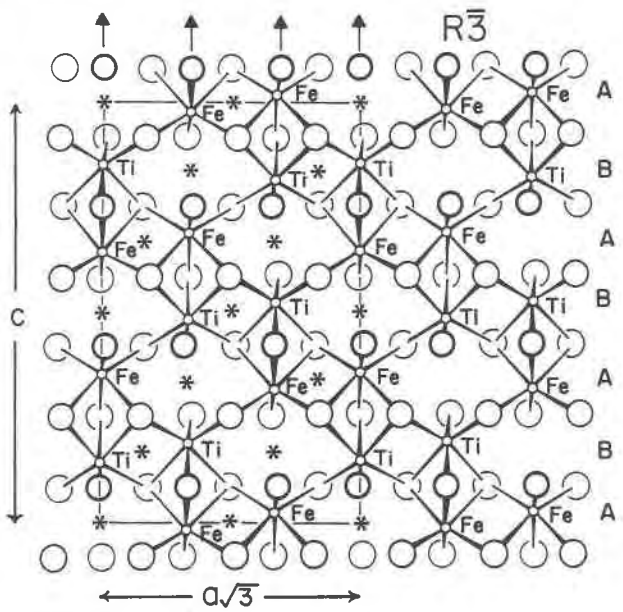

Fig. 3. Structure of $R\bar{3}$ ilmenite-hematite projected on to $(11\bar{2}0)$. This particular structure is of ordered ilmenite with an equal number of Fe and Ti cations. The cations are ordered onto alternating planes; by convention Fe lies on A planes and Ti on B planes. The twofold rotation axes in the triplets are lost during the transition because the common pair of cations are no longer equivalent. The remaining symmetry elements are the centers and the threefold axes parallel to **c**.

were heated in air at 620 °C in zero field for approximately 45 min, after which they were allowed to cool to room temperature in an applied field of 50 μT (0.5 Oe). Progressive AC demagnetization of the samples after acquisition of TRM was performed in AC fields up to 120 mT.

Structure of ilmenite-hematite

The solid solution between hematite, $R\bar{3}c$, and ilmenite, $R\bar{3}$, is characterized by a Fe-Ti order-disorder transition. The $R\bar{3}c$ structure represented by hematite and disordered ilmenite (Lindsley, 1976) consists of sheets of oxygen anions in a nearly hexagonal close-packed array lying parallel to (0001) (Fig. 2). Fe and Ti occupy the cation positions, as in the corundum structure. In pure hematite, Fe^{3+} is the only cation occupying these sites, whereas in high-temperature, disordered ilmenite-hematite solid solutions, Fe^{3+}, Fe^{2+}, and Ti^{4+} are randomly distributed over the cation sites. Groups of three oxygens called triplets form the common face of two adjacent octahedra, and each of these oxygens in the triplet is linked to the two cations in these octahedra (plus a third cation in a lateral edge-shared octahedron). In the $R\bar{3}c$ structure, these two cation sites are equivalent. A twofold rotation axis pierces the triplet and relates the common cations.

The $R\bar{3}$ structure is represented by ordered ilmenite-hematite solid solutions (Fig. 3). The octahedral cation positions are occupied as in the disordered form, but the cations are segregated onto alternating cation layers such that in pure ilmenite, layers contain only Fe^{2+} or only Ti^{4+}. With increasing hematite component, Fe^{3+} substitutes for Fe^{2+} and Ti^{4+} in both layers. By convention, the Fe-rich layer is termed the A layer, and the Ti-rich layer is termed the B layer. As an additional consequence of the cation ordering, the oxygens move away from the layers with the larger Fe cations and toward the layers with the smaller Ti cations. Both the cation ordering and the oxygen displacements destroy the **c**-glide and the twofold rotation and screw axes of the high-temperature, $R\bar{3}c$, disordered phase. Only the centers of symmetry and threefold axes remain. This symmetry loss results in the appearance of additional reflections of the type $h\bar{h}0l$, $l = 2n + 1$, in the ordered phase. The unit-cell size in both space groups is similar.

The magnetic structure of the ilmenite and hematite end-members and the intermediate solid solution is complex (Ishikawa, 1962; Lindsley, 1976). Above the magnetic ordering transition in Figure 1, all phases are paramagnetic. Below the magnetic ordering transition, the disordered $R\bar{3}c$ hematite and hematite-rich phases up to

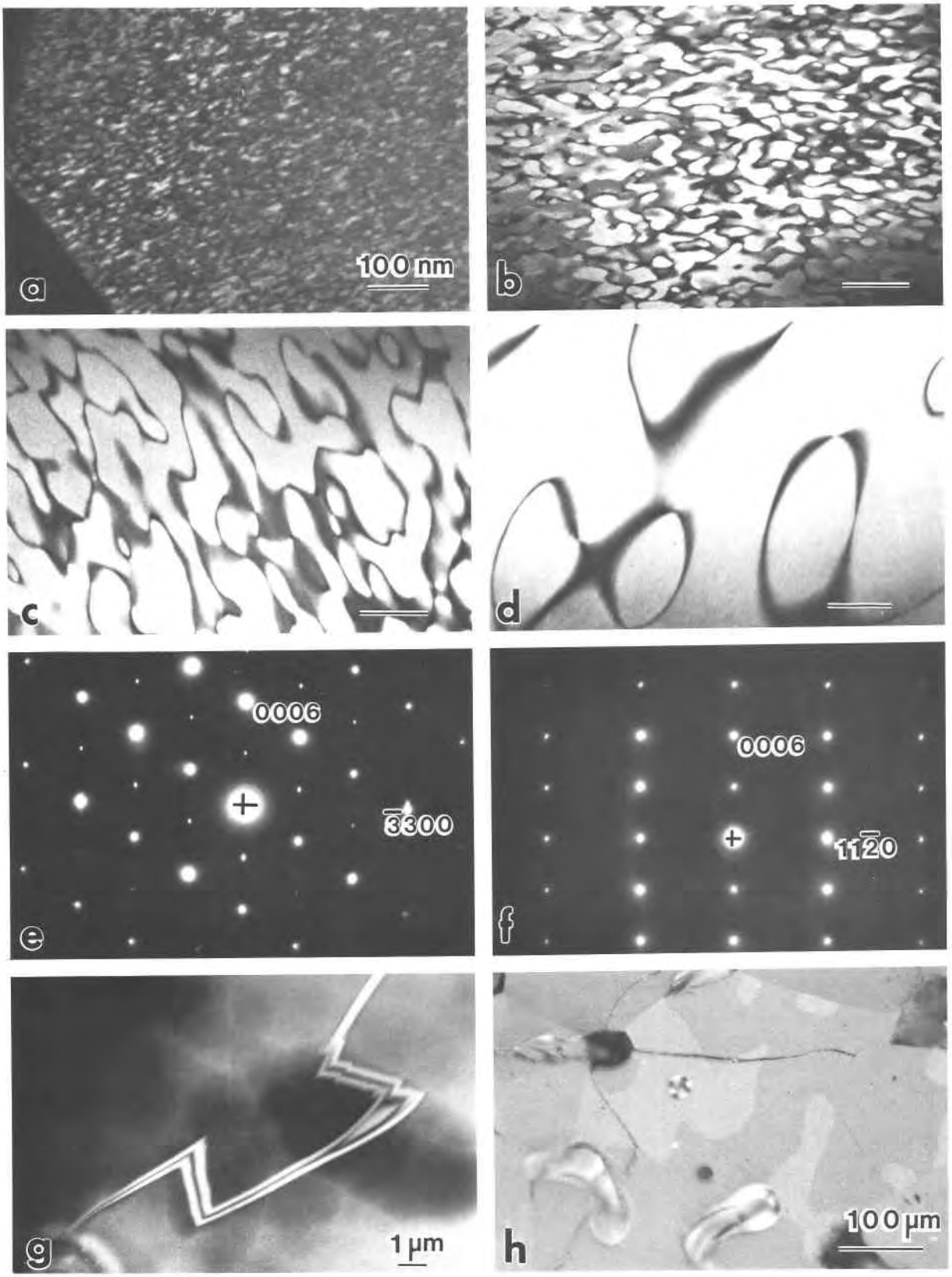
a
100 nm
b
c
d
e
0006
$\bar{3}300$
f
0006
$11\bar{2}0$
g
1 μm
h
100 μm

compositions of approximately Ilm_{45-50} are antiferromagnetic. In the disordered structure, Fe ions are randomly distributed on the different layers, so the total moment of each individual layer is the same. Coupling between adjacent layers is antiferromagnetic. The coupling, however, is imperfect, resulting in a weak parasitic ferromagnetic moment for the disordered phase of less than 1 emu/g. For samples with compositions between approximately Ilm_{50} and Ilm_{100}, the phases are of the ordered $R\bar{3}$ structure, and between Ilm_{50} and Ilm_{80}, they are ferrimagnetic at room temperature. Because the concentration of Fe on the A layers is greater than that on the B layers in ordered phases between Ilm_{50} and Ilm_{80}, the total magnetic moment due to A-layer contribution is greater than that due to B-layer contribution. This gives rise to a ferrimagnetic structure with room-temperature saturation magnetizations that can be greater than 30 emu/g. The transition between the weak parasitic ferromagnetic ordering and the strong ferrimagnetic ordering is somewhere in the range of Ilm_{45-55} and is highly dependent on the kinetics of the cation-ordering transition at higher temperatures as well as sample synthesis and thermal history. Compositions greater than Ilm_{80} remain magnetically disordered at room temperature and are thus paramagnetic. Short-range magnetic order and other complications do occur, but only below room temperature.

Transmission electron microscopy and reflected-light observations

Smoothly curving domain boundaries were observed by transmission electron microscopy in all synthetic ilmenites that were crystallized or annealed above the transition curve (Figs. 4a–4d). No domain boundaries were observed in those samples crystallized at temperatures below the transition. Coarsening of the domain microstructures was observed in samples that had been synthesized above and quenched through the transition and then subsequently annealed at temperature near but below the transition (Figs. 4g–4h). The domain boundaries are visible in dark-field images formed with the extra reflections that appear in the ordered phase, especially 0003 consistent with antiphase domain boundaries. However, it is also possible to see the domains clearly by a variation in background contrast between adjacent domains when using certain fundamental reflections (Fig. 5). This contrast is consistent with twin-domain boundaries. In order to determine the type of domain boundary by transmission electron microscopy, a contrast analysis of two-beam conditions with low-order reflections needs to be performed. This analysis is discussed in the next section.

If large enough, the domains are also visible optically when viewed in partially polarized reflected light in the petrographic microscope. They can be seen by a slight contrast difference (Fig. 4h) when the analyzer of the petrographic microscope is rotated several degrees from the polarizer. Under these conditions, the domains change contrast as the stage is rotated, and the domain microstructure is easily seen. This optical behavior is consistent with the domains having a twinning relationship.

Ilm_{65}, Ilm_{70}, and Ilm_{80} grown at 1300 °C and Ilm_{60} grown at 900 °C all have a domain microstructure (Fig. 4) indicating that they crystallized as the disordered phase and that the transition must lie below their crystallization temperature. Ilm_{90} and Ilm_{100} grown at 1300 °C and Ilm_{70} grown at 900 °C do not contain any domain boundaries, indicating that they crystallized as the ordered phase and that the transition lies above their crystallization temperature.

The shape of the domains varies from slightly flattened parallel to (0001) in Ilm_{60} and Ilm_{65} (these have the smallest domain size) to equidimensional in the more ilmenite-rich samples (these have progressively larger domain sizes). The flattening of the finest domains results in elongation of the $hk\bar{0}l$ ordering reflections parallel to **c** (Fig.4e). The domain size of Ilm_{65}, Ilm_{70}, and Ilm_{80} quenched from 1300 °C increases almost an order of magnitude for each additional 10 mol% ilmenite component. An additional 10 mol% ilmenite component increases the transition temperature by approximately 200 °C. Therefore, the domain size increase simply reflects an increase in diffusion rates with increasing temperature.

The transition was reversed for the composition Ilm_{70} by taking samples synthesized at one temperature and annealing them at another. Fine domains present in the 1300 °C quenched sample coarsened rapidly at 1000 °C, indicating that the transition is above 1000 °C for Ilm_{70}.

←

Fig. 4. Dark-field transmission electron micrographs of domain boundaries in quenched synthetic ilmenite-hematite solid solutions. (**a**) Ilm_{60} quenched from 900 °C showing very fine domains. (**b**) Ilm_{65} quenched from 1300 °C showing 300-Å average domain size. (**c**) Ilm_{70} quenched from 1300 °C showing 700-Å average domain size, and (**d**) Ilm_{80} quenched from 1300 °C showing domains greater than 1000 Å. All micrographs were taken at the same magnification with the ordering reflection **g** = 0003 at 120 keV (a and b) and 200 keV (c and d). (**e**) and (**f**) Electron-diffraction patterns for the zones $[11\bar{2}0]$ in Ilm_{60} and $[1\bar{1}00]$ in Ilm_{70}, respectively. In the $[11\bar{2}0]$ zone, the superlattice reflections ($hk\bar{0}l$, where $l = 2n + 1$) are weaker than the fundamental reflections and are slightly elongated parallel to **c** as a result of the flattened shape of the fine domains in Figure 4a. In the zone $[1\bar{1}00]$, only $000l$, $l = 2n + 1$ are superlattice reflections. These reflections, 0003 and 0009, would appear by double diffraction in this zone in any case. (**g**) Dark-field electron micrograph of coarsened domains in Ilm_{70} (**g** = 0003, 200 keV). This sample was crystallized at 1300 °C, quenched, and then annealed at 900 °C for 100 h. (**h**) Partially polarized, reflected-light micrograph of coarsened domains in Ilm_{70} that was quenched from 1300 °C and annealed at 1000 °C for 10 hr.

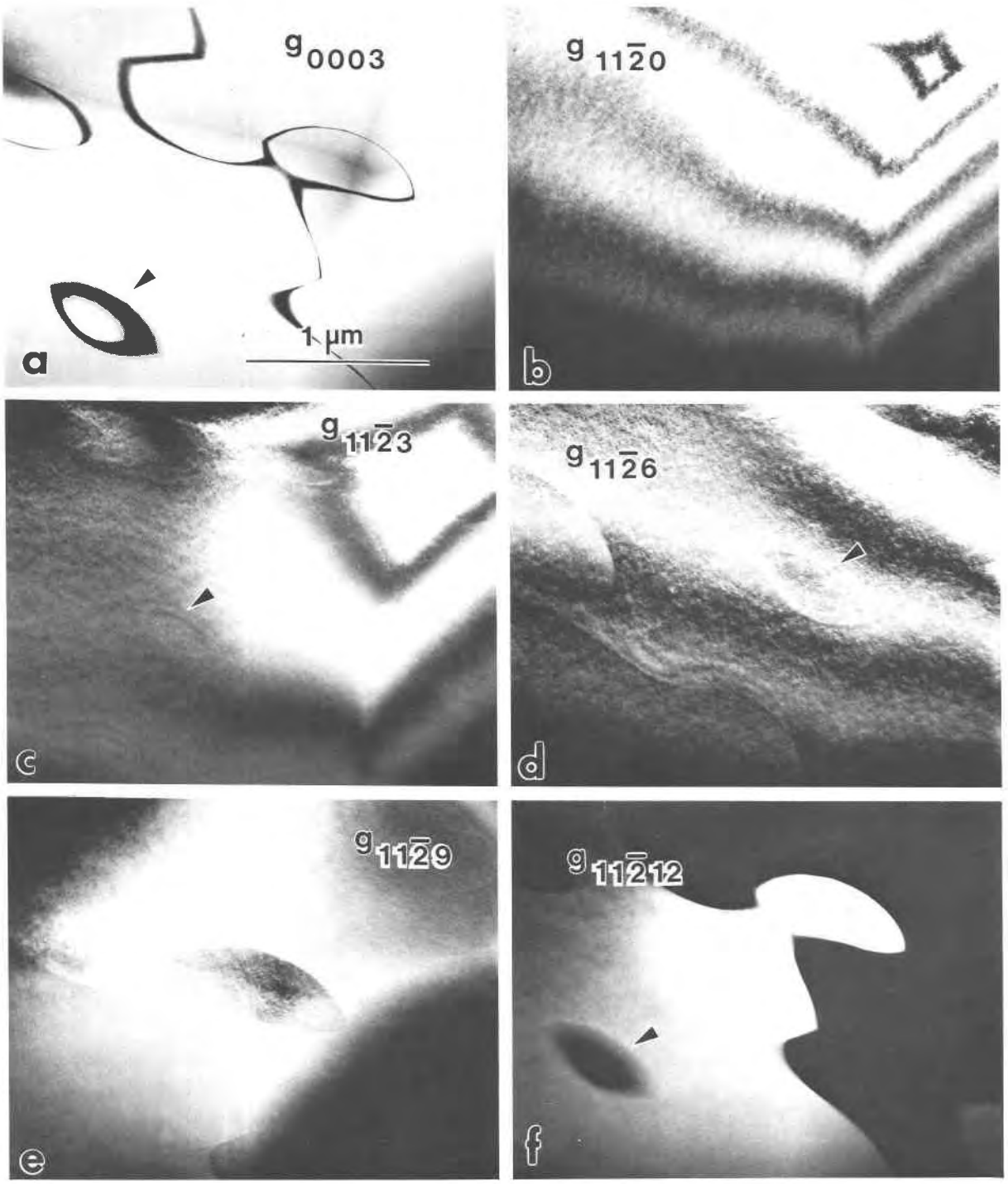

Fig. 5. Dark-field transmission electron micrographs of domain boundaries from the same area of Ilm_{70} annealed at 900 °C for 1 h. The operating reflections, **g**, indicated on each micrograph correspond to the [1$\bar{1}$00] diffraction pattern in Fig. 4f. An arrow on each micrograph indicates the position of the boundary of a single closed domain. All micrographs at 200 keV.

A portion of the 1000 °C sample with the coarsened domains was then annealed at 1050 °C for 10 h and quenched. It was found to contain fine domains, indicating that it had disordered at 1050 °C and re-ordered immediately upon quenching. Samples crystallized at 1300 °C and subsequently lowered to 1200, 1100, and 1050 °C and then quenched to room temperature contained progressively finer domains, indicating again that the tran-

sition lies below 1050 °C. The equililbrium transition, therefore, has been bracketed between 1000 and 1050 °C for Ilm_{70}.

Contrast analysis of cation-ordered domains and domain boundaries

The crystallographic relationship between adjacent domains can be determined from an analysis of the contrast of the domains and the domain boundaries under various diffraction conditions in the transmission electron microscope (Amelinckx and Van Landuyt, 1976, provide an excellent review). In general, two types of interfaces are developed as a result of an order-disorder transition: a translation interface and a twin interface. For ordering transitions that undergo a change in the size of the unit cell (formation of a superlattice), the domains are related by a translation vector that is a lattice vector of the disordered phase. For ordering transitions that result in the loss of a symmetry operation, the domains are related by a symmetry operation of the disordered phase. Amelinckx and Van Landuyt (1976) described the image contrast, extinction criterium, and effects on the diffraction pattern that are indicative of these different planar interfaces. The most pertinent for our quenched products is the fact that domains related by only a translation never show any contrast difference between domains whereas domains related by a twinning operation commonly show contrast differences between adjacent domains for many fundamental reflections. The domains in ordered hematite-ilmenite solid solutions show contrast differences and therefore must be related by a twin operation, and the domain boundaries must be twin interfaces. This is also consistent with the reflected-light observations.

In order to adequately describe the diffraction contrast of the twin-domain microstructure, we must construct a model that will account for all observations. The diffraction contrast of the domains and the domain boundaries is a function of the amplitude and phase of the operating reflections diffracted by each domain. Table 2 lists the calculated structure factors $|F_{hkil}|$ and phase angles (α) for given reflections *hkil* of the host and of the twin. In order to calculate the values for the twin, the atomic coordinates of the host were transformed by the relationship $X_T = Y_H$, $Y_T = X_H$, and $Z_T = 0.5 - Z_H$. This transformation relates the atomic coordinates of the host to the twin by a 180° rotation about an axis parallel to the **a** axis (two-fold axis in $R\bar{3}c$). Because the disordered ($R\bar{3}c$) and ordered ($R\bar{3}$) phases are centrosymmetric, the twin operation is a rotation and not an inversion.

The amplitude of the transmitted or diffracted electron beam exiting the specimen that forms an image by diffraction contrast is mainly a function of the deviation (s) from the exact Bragg angle and the extinction distance (ξ). The extinction distance is the critical distance in a perfect crystal over which the intensity of the diffracted beam varies from zero to some intensity and back to zero. The extinction distance depends on the operative reflection and may be calculated from the relationship (Hirsch et al., 1965)

$$\xi = (\pi V_c \cos\theta)/(\lambda F_{hkil}),$$

where V_c is the unit-cell volume, θ is the Bragg angle, and λ is the electron wavelength calculated at the operating voltage of the TEM.

Table 2. Extinction distances in ordered ilmenite

	h	*k*	*i*	*l*	Structure factor	α (°)	ξ (Å)	ξ_{g^1}/ξ_{g^2}
Host	0	0	0	3	5.53	180	7147	1.0
Twin	0	0	0	3	5.53	0	7147	
Host	0	0	0	6	29.45	180	1342	1.0
Twin	0	0	0	6	29.45	180	1342	
Host	0	0	0	9	10.38	0	3809	1.0
Twin	0	0	0	9	10.38	180	3809	
Host	0	0	0	12	24.70	0	1600	1.0
Twin	0	0	0	12	24.70	0	1600	
Host	1	1	$\bar{2}$	0	24.40	0	1620	1.0
Twin	1	1	$\bar{2}$	0	24.40	0	1620	
Host	1	1	$\bar{2}$	3	59.96	0	659	0.82
Twin	1	1	$\bar{2}$	3	49.04	0	806	
Host	1	1	$\bar{2}$	6	44.30	0	892	0.75
Twin	1	1	$\bar{2}$	6	58.61	0	674	
Host	1	1	$\bar{2}$	9	31.92	180	1238	0.69
Twin	1	1	$\bar{2}$	9	21.93	180	1802	
Host	1	1	$\bar{2}$	12	4.62	180	8558	0.26
Twin	1	1	$\bar{2}$	12	17.95	180	2202	

Note: 200 keV, $s = 0$.

Extinction distances in Table 2 were determined for pure ordered ilmenite with electron scattering factors from Smith and Burge (1962) and atomic positions from Raymond and Wenk (1971). These distances are applicable only for the exact Bragg position where $s = 0$ and are only accurate to within 10%, primarily because of uncertainty in the electron scattering factors.

The data in Table 2 can be compared to dark-field two-beam observations in the transmission electron microscope for the zone [1$\bar{1}$00] (Fig. 5).

For **g** = 0003, we find that $F_H\{0003\} = F_T\{0003\}$ and that the difference in the phase angles is 180°. Therefore both domains should show the same intensity, and the domain boundaries should exhibit the fringe contrast of a π fault (Fig. 5a). Because the extinction distance for {0003} is large, almost 0.75 μm, only the central dark fringe is visible in micrographs taken in thin areas. Figure 4g of the 900 °C, 100-h anneal, however, was taken in a thicker area at low magnification and a central black fringe bordered by white fringes can be seen. This is typical of the dark-field symmetry of π fringes. Similarly, for **g** = 0009, symmetrical fringes are visible at the boundary, and the domains have identical diffraction contrast.

For **g** = 0006 we find that $F_H\{0006\} = F_T\{0006\}$ and that the difference in the phase angles is zero. Both do-

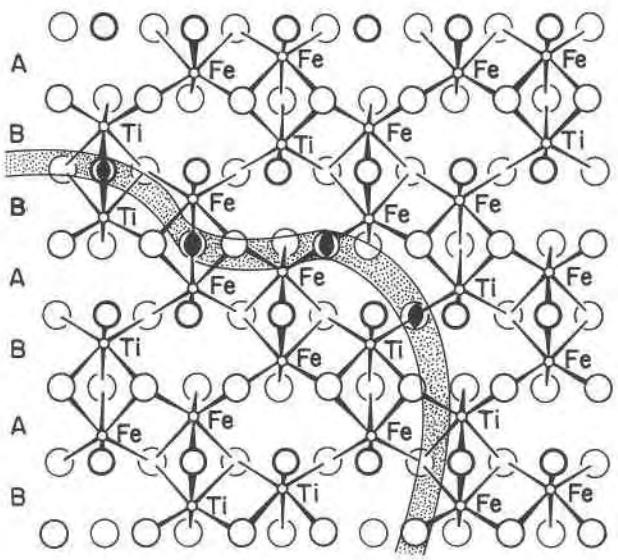

Fig. 6. Transition-induced twin-boundary model. Projection of the crystal structure of Ilm_{70} on to $(11\bar{2}0)$. For this composition, approximately 7.7 of the cations are Fe and 4.3 are Ti per unit cell. During cation ordering, the right side of the model ordered on an A-B scheme while the left side ordered on a B-A scheme, where A layers contain only Fe and B layers contain Fe and Ti. Upon growth and impingement of the two ordered domains, a twin boundary is developed (stippled band). The domains are related by a twofold axis at the boundary represented by the filled oxygens. A 180° rotation about these axes will bring the A and B layers as well as the oxygen lattice back into register.

mains should show the same intensity, and the boundary should not be visible. This is in fact observed. Similarly, for $\mathbf{g} = 0.0.0.12$ and $11\bar{2}0$ (Fig. 5b), no boundary contrast is visible, and the domains have identical contrast.

For $\mathbf{g} = 11\bar{2}3$, we find that $F_H\{11\bar{2}3\} \neq F_T\{11\bar{2}3\}$, but that the difference in the phase angles is zero. In this situation, adjacent domains should show an intensity difference for a crystal of constant thickness, and the boundaries should not show fringe patterns. Images using $\mathbf{g} = 11\bar{2}3$ (Fig. 5c) show thickness contours that are offset when they cross the domain boundaries, indicating a change in extinction distance between the two simultaneously operating reflections from the host and twin. The boundary is barely visible with weak fringes in thicker areas. The reflections $11\bar{2}6$, $11\bar{2}9$, and $1.1.\bar{2}.12$ also give unequal structure factors between the host and twin. The ratio of the extinction distance between that of the host and that of the twin decreases as l increases, and we would therefore expect that the domains will show increasing diffraction-contrast differences as l increases. This is observed in the images (Figs. 5d–5f). In fact, the extinction distances for $\mathbf{g} = 1.1.\bar{2}.12$ are so different as to permit a black-white intensity difference between the domains. In this set of images, the domain boundary shows a weak fringe contrast. McLaren and Phakey (1969) showed for Dauphiné twins in quartz (also 180° rotation twins) that the weak fringes in the boundary do not arise from any phase difference or misorientation between the twins but from the fact that the extinction distances in the two twins are widely different.

Twin-domain boundary model

The twin-domain boundaries form during cooling through the order-disorder transition. At high temperature, Fe and Ti are disordered over the cation sites. As the transition temperature is approached, small ordered areas began to form with Fe concentrating on one layer and Ti on the adjacent layers. These areas can order in- or out-of-phase with adjacent ordering areas. If adjacent areas order in-phase, then upon growth and impingement, a perfect match is achieved and no boundary results. If the adjacent areas order out-of-phase, then upon growth and impingement, Fe-rich layers abut Ti-rich layers and vice versa. Figure 6 illustrates such a case for ferrian ilmenite with a bulk composition of Ilm_{70}. The A and B cation layers of one ordered domain are out-of-phase with the A and B layers of the adjacent ordered domain. The stippled boundary between the domains has its own local symmetry. Twofold rotation axes that were present in the disordered phase are retained in the boundary. Rotation of 180° about any one of the filled oxygens will bring the A and B cation layers of the adjacent domains into register. Thus, the model boundary is a twin boundary as required by the diffraction-contrast experiments.

The twin-boundary model in Figure 6 provides some insight into the properties of the boundary. (1) The boundary represents a ribbon of disordered $R\bar{3}c$ phase because of the presence of the $R\bar{3}c$ symmetry elements. This implies that the boundary region should consist of a weak, parasitic, ferromagnetic moment similar to a disordered hematite-rich phase, in contrast to the ferrimagnetic cation-ordered domains. (2) The boundary is locally enriched in Fe or Ti. If the adjacent layers are both A layers, the boundary is enriched in Fe, which results in a ribbon of magnetic phase with a higher Curie temperature than the ordered domains. There is some independent evidence for Fe enrichment of the boundaries. Hoffman (1975a) found that the blocking temperature of the "x" phase in Ilm_{60} was approximately 340 °C, which corresponds to approximately Ilm_{40-45}. (3) The boundary has a surface energy because of lattice strain. Ordering of Fe and Ti on adjacent layers causes the nearly close-packed oxygen layers to move toward the Ti-rich layer and away from the Fe-rich layer because of the difference in atomic radius of the two cations. This adjustment of the distances between layers must reverse itself upon crossing a twin-domain boundary. The strain between the two domains will be maximum for boundary orientations parallel to **c** and a minimum for boundary orientations parallel to the basal plane. Thus the domains are expected to be flattened parallel to the basal plane as seen in Figure 4. This flattening is confirmed by the elongated ordering reflections in selected-area electron diffraction patterns of fine-grained twin domains.

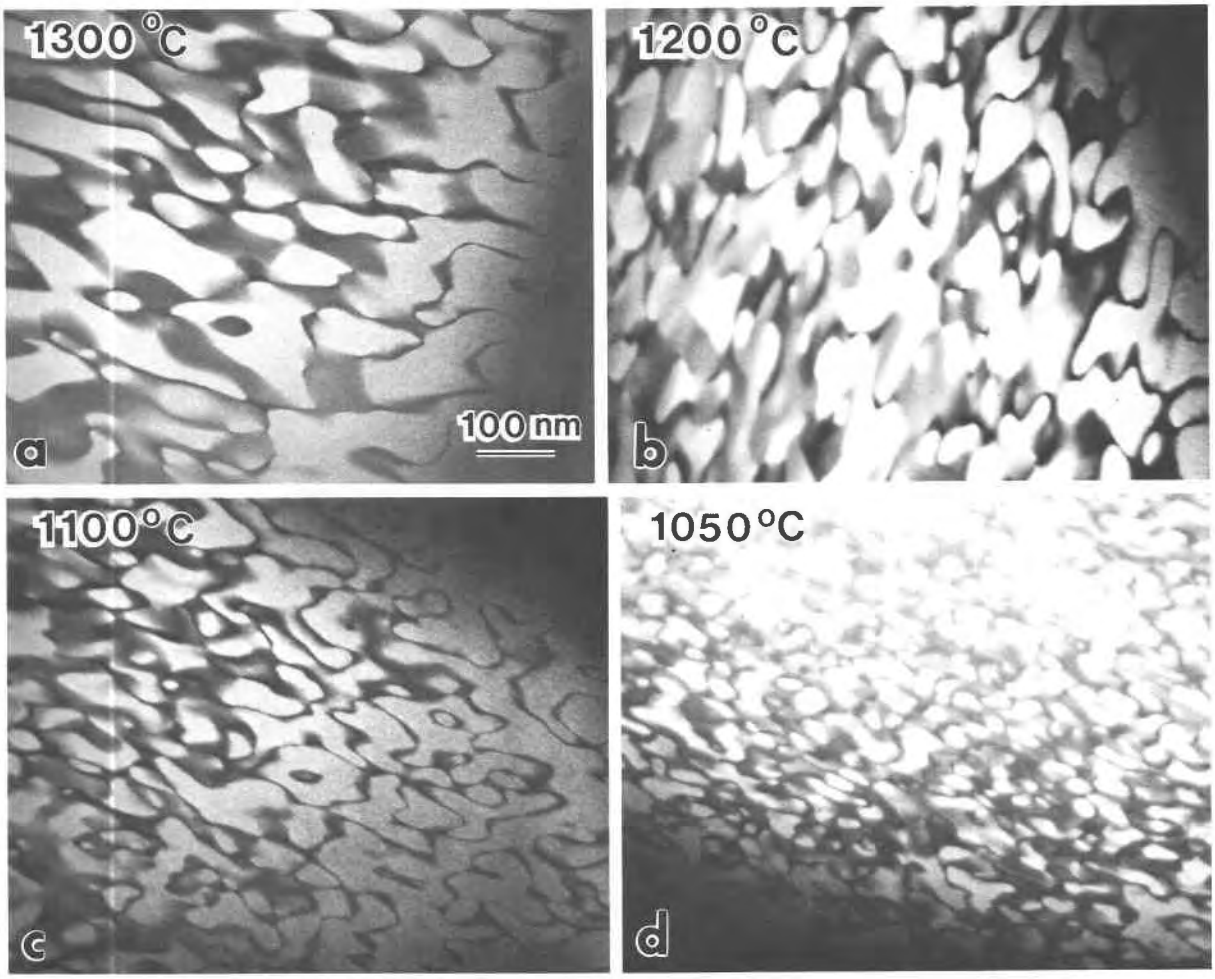

Fig. 7. Dark-field transmission electron micrographs of domain microstructures in Ilm_{70} quenched from temperatures progressively closer to the transition temperature at approximately 1025 °C. Each sample was crystallized at 1300 °C for 48 h, and then the furnace temperature was reduced to the annealing temperature indicated on the micrographs; the gas-mixing ratio was held constant. The samples were annealed for 10 h and then quenched into liquid N_2. The resulting domain size is reduced by a factor of two as T_c is approached.

Variation of domain size with quench temperature

The size of the twin domains that arise from cooling through the order-disorder transition progressively decreases as the quench temperature approaches the transition temperature. Figure 7 shows electron micrographs of twin domains in Ilm_{70} samples that were quenched from 1300, 1200, 1100, and 1050 °C; mean domain diameters are 706, 633, 520, and 370 Å, respectively. Each sample was synthesized at 1300 °C, and then the furnace temperature was lowered while maintaining the same CO_2/H_2 ratio of 99. The samples were then held for 10 h to equilibrate at the lower temperature before quenching to room temperature. At temperatures below 1200 °C, the buffering gases trended off the equilibrium curve and became slightly more reducing than the calculated equilibrium value. At 1050 °C, the oxygen fugacity was approximately 0.5 log unit more reducing than the equilibrium value. However, examination of the quenched samples indicated that no spinel phase was formed.

There are a number of possible explanations as to why the domains formed from higher quench temperatures are larger. (1) The high-temperature quenches are at sub-T_c temperatures for a longer period of time, allowing coarsening of finer domains. (2) Greater vacancy concentrations occur at the higher temperatures and thus increase diffusivities at T_c. (3) Short-range order (SRO) just above the transition temperature provides abundant clusters of the ordered phase, providing a higher density of ordering sites and consequently forming finer domains. The further the quench temperature is above T_c, the weaker the SRO clustering. (4) Diffusivity is a function of oxygen fugacity, and the lower-temperature quenches are more reducing. Any of these explanations or a combination of them are possible causes for the decrease in

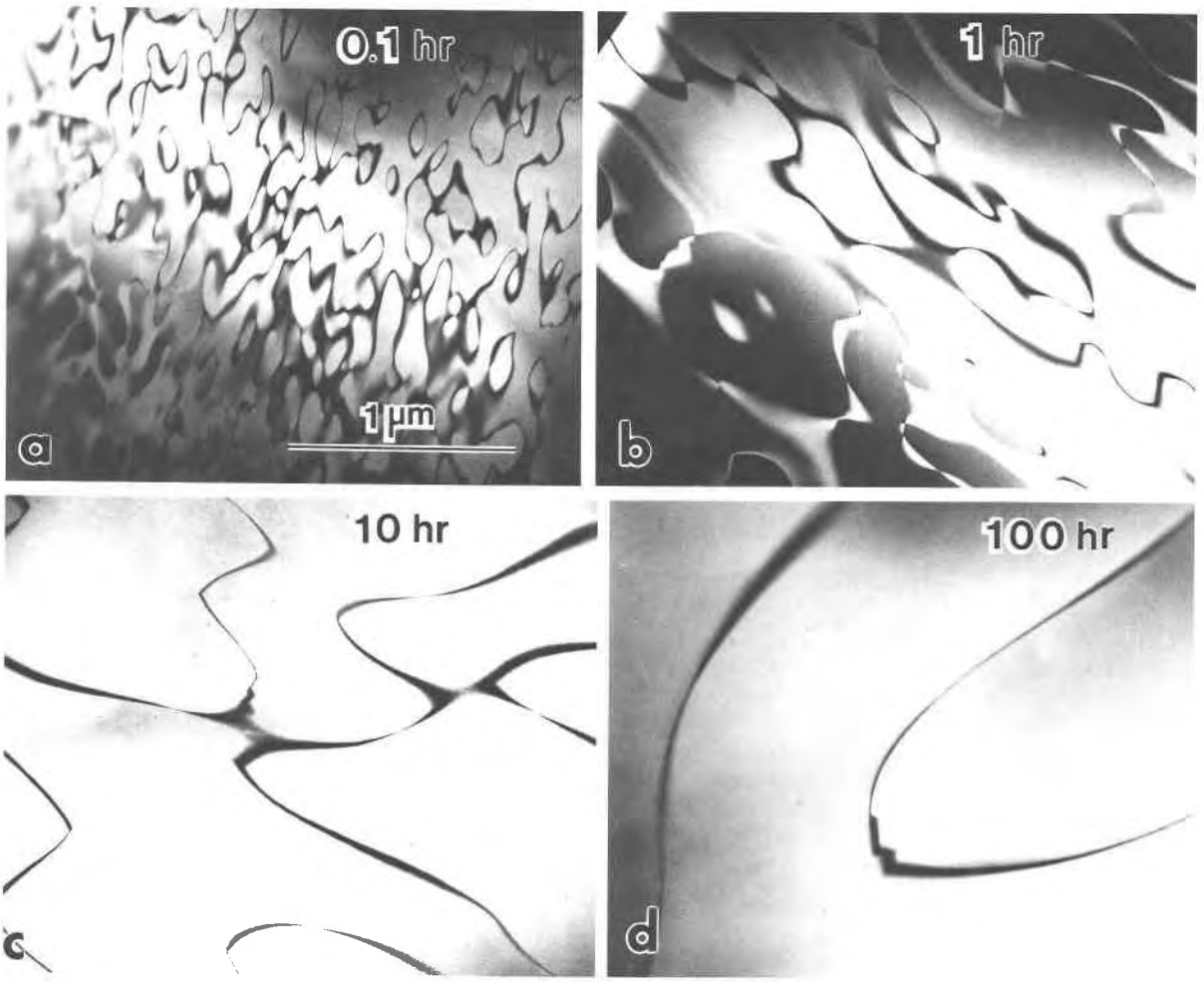

Fig. 8. Dark-field transmission electron micrographs of Ilm_{70} annealed at 800 °C for (**a**) 0.1 h, (**b**) 1.0 h, (**c**) 10.0 h, and (**d**) 100.0 h. **g** = 0003 in all micrographs.

domain size with quench temperature; the fact that the decrease exists is important when understanding the magnetic properties and extrapolating the properties of the synthetics to natural ferrian ilmenite occurrences.

Coarsening kinetics and morphology of the twin domains

The surface energy of the twin-domain boundaries is due to lattice strain at the boundary. This surface energy is reduced by reducing boundary area or aligning the boundary along orientations of minimal strain. Boundary area is reduced by enlarging or coarsening the domains. The kinetics of domain coarsening were studied by annealing quenched samples, with a fine initial domain microstructure, in the single-phase field below the order-disorder transition. Nord and Lawson (1988) found that the domains coarsen according to the relationship $D^n = kt$ where $n = 2.44$, D is the domain diameter, k is a rate constant, and t is time. The activation energy for coarsening was found to be 77 kcal/(deg·mol) [321 kJ/(deg·mol)]. The fact that the coarsening rate does not follow a parabolic law ($n = 2$) is attributed to nonstoichiometry and possibly to concentration of vacancies on the boundary.

The increases in domain size during the coarsening experiments are given in Table 3 where the domain diameters were determined by the previously described intercept method. The domains coarsen by straightening out curved boundaries and forming small totally enclosed domains that shrink and disappear. These small domains can be seen in Figure 5 where they form football shapes with the long dimension parallel to (0001). Figure 5a also shows a good example of a domain in the process of pinching off from a larger domain. This domain will shrink and disappear with further annealing below T_c. During the coarsening process, the domain boundaries also appear to orient themselves along rhombohedral planes. Figure 8 illustrates this in a sequence of annealing runs at 800 °C. Unfortunately, the orientation is not developed enough to determine it exactly. The strong curvature and steplike surface of the domain as it swings through planes parallel to **c** certainly indicates a high boundary energy in

TABLE 3. Microstructure and magnetic intensity of Ilm_{70}

Run	Thermal history	Average domain size* (Å)	Boundary area ($\times 10^6$ m^2/m^3)	Saturation magnetization (emu/g)
70,02,00	1300 (37 h), Q	706 ± 54	28.3 ± 2.2	30.5 ± 0.6
70,20,00	1300 (67 h) to 1200 (10 h), Q	630 ± 50	31.6 ± 2.5	29.3 ± 0.3
70,21,00	1300 (41 h) to 1100 (10 h), Q	520 ± 50	38.3 ± 2.5	26.8 ± 0.5
70,23,00	1300 (46 h) to 1050 (10 h), Q	370 ± 50	54.5 ± 2.5	26.1 ± 0.4
70,29,00	1300 (41 h) to 1000 (10 h), Q	2000000	0.02 est.	30.9 ± 0.3
70,22B,00	1300 (41 h) to 1000 (10 h), Q to 1050 (10 h), Q	n.d.	n.d.	n.d.
	Runs annealed in silica-glass tubes for the duration indicated‡			
70,14B,01	900 (0.1 h), Q	5074 ± 214	3.9 ± 0.2	34.2 ± 0.8
70,04B,01	900 (1 h), Q	11992 ± 4004	1.8 ± 0.6	35.4 ± 0.6
70,07B,01†	900 (10 h), Q	11749 ± 2248	1.8 ± 0.4	28.9 ± 0.8
70,02B,01	900 (100 h), Q	350000 est.	0.06 est.	36.0 ± 0.3
70,32B,01	800 (0.1 h), Q	n.d.	n.d.	32.4 ± 0.7
70,15B,01	800 (0.1 h), Q	1296 ± 98	15.4 ± 1.2	31.7 ± 1.2
70,05B,01	800 (1 h), Q	3752 ± 292	5.3 ± 0.3	32.7 ± 1.4
70,08B,01	800 (10 h), Q	8293 ± 713	2.4 ± 0.2	34.6 ± 0.3
70,12B,01	800 (100 h), Q	25008 ± 6272	0.8 ± 0.2	35.7 ± 0.2
70,30B,01	700 (0.1 h), Q	n.d.	n.d.	30.8 ± 0.5
70,06B,01	700 (1 h), Q	876 ± 66	22.9 ± 1.7	31.8 ± 0.2
70,09B,01	700 (10 h), Q	2084 ± 132	9.2 ± 0.6	33.4 ± 0.1
70,33B,01	700 (10 h), Q	n.d.	n.d.	32.8 ± 0.9
70,11B,01	700 (100 h), Q	5086 ± 754	3.5 ± 0.4	34.1 ± 0.6
70,16B,01	700 (1000 h), Q	11944	1.7	35.5

Note: n.d. = no data. Q = quench.
* Plus or minus 1σ standard deviation.
† Magnetite precipitated in this run during annealing.
‡ The starting materials were synthesized at 1300 °C in the gas-mixing furnace.

those orientations. The steps are rhombohedral planes parallel to $\{\bar{1}104\}$ and $\{1\bar{1}02\}$, and their presence minimizes the boundary surface energy.

TWIN-BOUNDARY SURFACE AREA, ANNEALING TIME, AND SATURATION MAGNETIZATION

Ishikawa (1958) showed that the room-temperature saturation magnetization, J_s, of quenched ilmenite-hematite solid solutions is dependent on the degree of cation order. The disordered $R\bar{3}c$ phase has a weak magnetic moment, whereas the ordered $R\bar{3}$ phase has a strong magnetic moment. In addition, J_s decreases when the quench temperature approaches the order-disorder transition. This is because the degree of long-range order in the cation-ordered domains decreases as T_c is approached. The Ilm_{70} microstructure shown in the previous figures contains both disordered domain boundaries and ordered domains. Therefore, the room-temperature saturation magnetization (J_s) of quenched Ilm_{70} will depend on the volume percent of disordered twin-domain boundary and ordered domains as well as the degree of long-range order in the domains themselves. Because we cannot measure the thickness of the domain boundary, we cannot determine the volume ratio; however, the twin-boundary surface area per unit volume (S_V) can be measured. S_V and J_s are tabulated in Table 3 for all samples. Figure 9a shows that S_V decreases with increasing annealing time, which is expected because of domain coarsening. It also shows that the reduction in S_V is much faster at higher temperatures where diffusion rates are higher. Figure 9b shows that as S_V decreases, J_s increases. This trend is also expected because the TEM study indicates that the twin-domain boundaries are ribbons of the disordered phase and therefore will have a weaker J_s than the ordered phase. As the volume of the disordered boundary phase de-

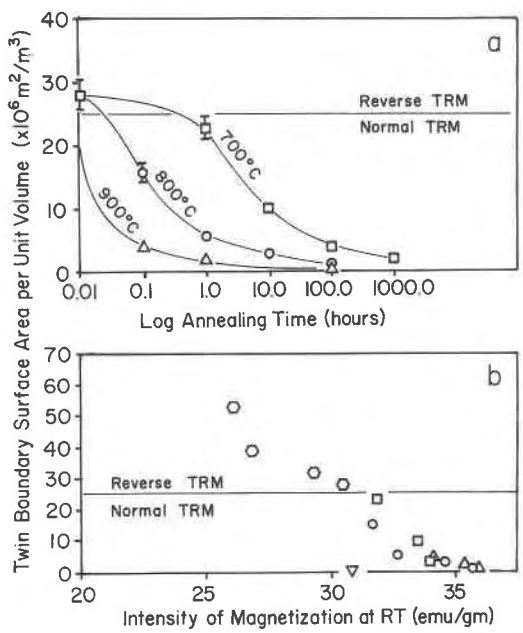

Fig. 9. (a) Twin-boundary surface area versus log annealing time. (b) Twin-boundary surface area versus room-temperature saturation magnetization. Symbols are as in (a); the 1000 °C anneal is an inverted triangle, and the four samples quenched from above T_c are hexagons.

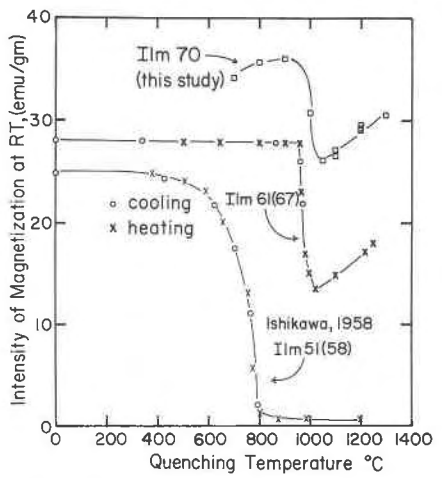

Fig. 10. Intensity of magnetization measured at room temperature versus quenching temperature.

creases, the volume of the ordered, higher-J_s phase increases. Increases in the degree of order within the domains themselves with longer annealing times will also contribute to the increase in J_s.

The horizontal line at a twin-boundary surface area of approximately 25×10^6 m^2/m^3 in Figures 9a and 9b separates samples that exhibit a reverse TRM and samples that exhibit a normal TRM. All of the Ilm_{70} samples quenched through the transition have a reverse TRM. However, short annealing times, even at 700 °C, are sufficient to reduce the boundary surface area and consequently destroy the self-reversing capability. The 0.1-h anneal at 700 °C was found to self-reverse, but no boundary areas have been measured. After 1-h annealing at 700 °C, the samples become normal.

It is not possible to separate the contribution to the saturation magnetization (J_s) due to the disordered domain boundaries and that due to the long-range cation order in the domains. As the cation-ordered transition temperature is approached from below, the degree of long-range cation order decreases slowly and then rapidly to zero at the transition temperature, T_c. Figure 10 shows a graph of room-temperature magnetization versus the quench temperature for our experiments with Ilm_{70} and Ishikawa's experiments with $Ilm_{61(67)}$ and $Ilm_{51(58)}$. (We actually believe his compositions are closer to Ilm_{67} and Ilm_{58}, as explained in the next section; thus the values in parentheses.) For both studies, the samples plotted in Figure 10 were annealeld at temperature for some period of time and quenched. The curves for the Ilm_{70} and $Ilm_{61(67)}$ data sets show a steep drop in magnetization at the transition, whereas the $Ilm_{51(57)}$ curve shows a gradual drop to very low values for the high-temperature quenches. The lower-temperature quenches reflect equilibration in the cation-ordered $R\bar{3}$ field, and the high-temperature quenches reflect equilibration in the cation-disordered $R\bar{3}c$ field. The difference between the shape of the curves is due to the 200 °C difference in transition temperature; 1000–1050 °C for Ilm_{70} and 800 °C for $Ilm_{51(58)}$. The higher-transition-temperature quenches were able to order significantly during quench (Fig. 7), whereas the lower-transition-temperature quenches (Fig. 4a) were not. Therefore, the $Ilm_{51(58)}$ curve follows the expected Bragg-Williams approximation, whereas disorder in the more ilmenite-rich compositions is more difficult to quench.

Particularly interesting is the area above the transition where the magnetization increases with increasing quench temperature for Ilm_{70} and $Ilm_{61(67)}$. Ishikawa (1958) suggested that samples were able to partially reorder, thus resulting in an increase in the magnetization. In fact, our series of experiments quenched from 1300, 1200, 1100, and 1050 °C shows that the disordered phase is not quenchable. The selected-area diffraction patterns all give strong and sharp ordering reflections from the ordered $R\bar{3}$ phase. What is apparent is that the amount of disordered domain boundary is higher in the samples quenched from temperatures just above T_c (Figs. 7, 9b, and Table 3). The samples quenched closest to T_c, therefore, would be expected to have lower magnetization values. The magnetization trend above T_c will also depend on the ability of the ordered domains to approach the fully ordered configuration. The kinetics of ordering will be affected by any variation in stoichiometry and any difference in the rate of heat loss during quench. Our samples were not encapsulated and were quenched directly into liquid N_2, whereas Ishikawa's samples were contained in a quartz tube and were quenched into brine. The two curves are very similar in form, the only difference being the magnitude of the intensity. Ishikawa (1958) made his measurements at 8000 Oe, whereas our J_s values were calculated by extrapolating to infinite field. These differences in experimental techniques can account for the difference between the two sets of curves. The 700 and 800 °C anneals show decreasing magnetization as the annealing temperature is decreased, whereas the samples of Ishikawa show a constant intensity at the lower temperatures. This is the direct result of the thermal history of our samples. The lower-temperature anneals have a larger domain surface area (Table 3) and thus lower magnetization intensity. We cannot evaluate Ishikawa's samples annealed below T_c because the total thermal histories are not known.

The sample annealed at 1000 °C has a twin domain size of over 100 μm, large enough to be visible in reflected light. We would expect the J_s of this sample to be the highest of all the ordered samples because of the very low boundary area. However, it has a J_s of 31 emu/g, whereas the samples annealed at lower temperatures with much higher boundary surface areas have higher saturation magnetizations. We believe we have quenched in some long-range cation disorder that was present in the sample while it was annealed just below T_c. This cation disorder manifests itself by reducing the room temperature J_s.

Determination of the $R\bar{3}c$ to $R\bar{3}$ transition

The first determination of the order-disorder transition in ilmenite-hematite solid solutions was made by Ishikawa (1958). He measured the room temperature mag-

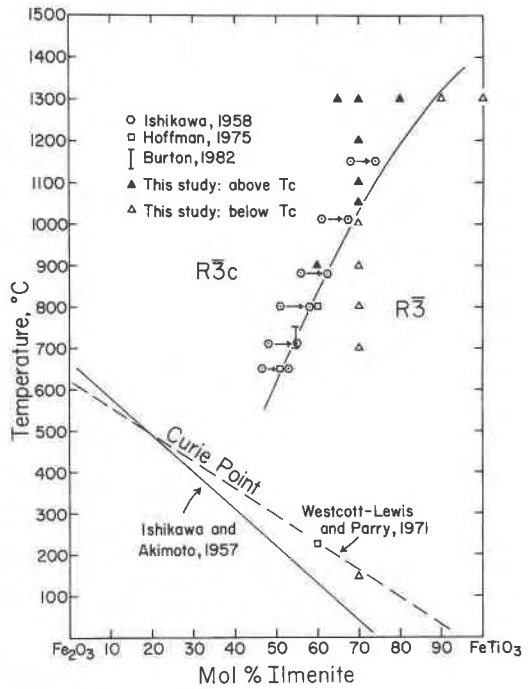

Fig. 11. Fe_2O_3-$FeTiO_3$ phase diagram showing the fields of $R\bar{3}c$ and $R\bar{3}$. The filled triangles indicate the composition and crystallization temperature of synthetic samples that contained domain boundaries after quenching. The open triangles indicate samples that did not contain domain boundaries after quenching or showed coarsening of pre-existing domains. The results from earlier studies are discussed in the text. The order-disorder transition is drawn as a single line.

TABLE 4. Experimental data for $R\bar{3}c$ to $R\bar{3}$ transition

Ilm (mol%)	T_c (°C)	Ilm (mol%)	T_c (°C)
		Redetermined using Lindsley's (1965) volume vs. composition curve	
	Ishikawa (1958)*		
46.5	~650†	53	~650
48	710	55	710
51	800	58	800
56	880	62.5	880
61	1010	67.5	1010
68	1150	74	1150
	Hoffman (1975a)		
51	~650‡		
60	800§		
	Burton (1982)		
54.6	$700 < T_c < 750$		
	This study		
60	<900		
65	<1300		
70	$1000 < T_c < 1050$		
80	<1300		
90	>1300		
100	>1300		

* T_c taken as change in slope on diagrams of intensity of magnetization vs. temperature in Ishikawa (1958).
† Appears to be a smeared transition.
‡ "$X = 0.51$ . . . near 650 °C," p. 76.
§ "$T_q = 800$ °C" and Fig. 5, p. 72.

netization of synthetic samples that had been annealed at a constant temperature and then quenched into brine (Fig. 10). Ishikawa equated the decrease in magnetization with the long-range order parameter, S, and placed the transition temperature, T_c, at the change in slope or where the long-range order parameter reached a minimum. From his plots of magnetization versus quenching temperature, we have plotted T_c for six compositions on Figure 11.

Hoffman (1975a) determined a T_c for Ilm_{60} at 800 °C and Ilm_{51} near 650 °C. Even though he determined T_c using the same magnetic measurements, his values are several hundred degrees below those of Ishikawa. Burton (1982) determined T_c for Ilm_{54} to lie between 700 and 750 °C by observing the change in intensity of an ordering reflection during in situ heating on a single-crystal diffractometer. This value is consistent with Hoffman's determinations but again is several hundred degrees below that of Ishikawa's. Both Hoffman and Burton's determinations for T_c fit on the transition bracketed by the behavior of the transition-induced domains (Fig. 11 and Table 4).

The key to the disrepancy between Ishikawa's data points and those of Burton, Hoffman, and this study lies in understanding how the sample compositions were determined. Nagata and Akimoto (1956) determined that the $FeTiO_3$ content of the hematite-ilmenite solid solution is related in a linear fashion to the volume of the unit cell (Fig. 12). The compositions of their synthetic solid solutions of ilmenite-hematite were determined by chemical analysis, but the analytical totals ranged from 89% to 100%. Ishikawa and Akimoto (1957, p. 1085), assuming that the empirical linear composition-volume relationship was correct, determined the chemical composition of specimens used for the order-disorder study only by X-ray diffraction. Subsequently, Ishikawa (1958) also used the unit-cell volumes to determine the mole fraction of $FeTiO_3$. However, it was shown by Lindsley (1965) that the cell volumes show a negative deviation from the linear relationship (Fig. 12). Subsequent work by Hoffman (1975a) and Lawson (1981), where cell volumes were determined on samples that were also analyzed by the electron microprobe, agreed with the volume versus composition curve of Lindsley. The deviation of the volume from ideality is not trivial. For instance, the correction for Ilm_{56} determined from the linear relationship to a composition determined from Lindsley's curve would be approximately 7 mol% or a corrected value of Ilm_{63}. In Figure 11 and Table 4, we have corrected Ishikawa's data points by determining the composition as it would fall on Lindsley's curve. The transition curve drawn is now a reasonable fit for all the data points and brackets from the four studies of the transition critical temperature.

The Curie points determined by Ishikawa and Akimoto (1957) can be treated the same way. The Curie point trends for both Ishikawa and Akimoto (1957) and later determinations by Westcott-Lewis and Parry (1971a) along with points for Ilm_{60} by Hoffman (1975a) and Ilm_{70} from this study are plotted in Figure 11. Again, the dis-

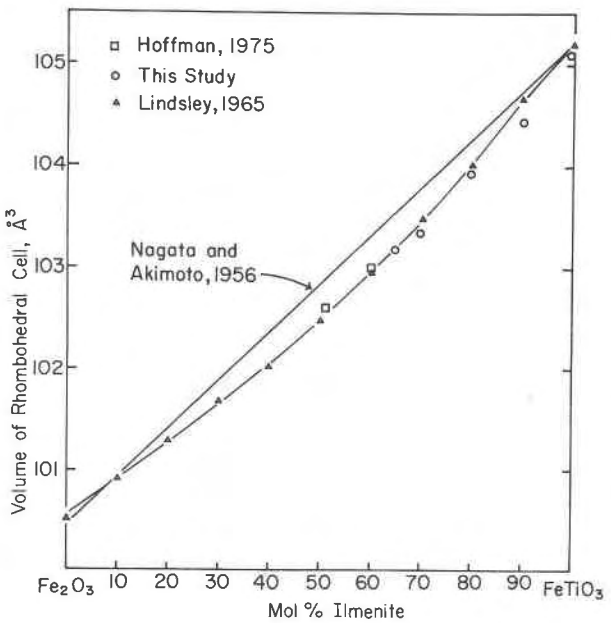

Fig. 12. Volume of the rhombohedral unit cell of ilmenite-hematite solid solutions. This figure compares the linear volume versus composition relationship suggested by Nagata and Akimoto (1956) with that determined by Lindsley (1965). Synthetics from this study and those of Hoffman (1975a) lie on Lindsley's volume-composition curve.

crepancy between the two sets of data can be reduced by correcting Ishikawa's sample compositions.

Applications to natural ferrian ilmenites

Natural ferrian ilmenites exhibiting self-reversed TRM have been found mainly in dacitic tufts. The compositions range from Ilm_{53} to Ilm_{65} and have crystallization temperatures between 850 and 950 °C (Lawson et al., 1987). This temperature-composition range lies above the order-disorder curve in Figure 11. Within this range lies the Ilm_{60} synthetic sample that was crystallized at 900 °C. This sample was found to be self-reversing (Lawson, 1981) and to contain a 100-Å twin domain microstructure (Fig. 4a). Two natural self-reversing ferrian ilmenites have been examined by us in the TEM, and both were found to contain a similar fine twin-domain microstructure. One was an Ilm_{58-59} from a dacitic pumice block at Mount Shasta, California (Fig. 9, in Lawson et al., 1987), and the other was an Ilm_{55-59} from a dacite at White River, Alaska (Lerbekmo et al., 1975).

The similarity between the natural and synthetic ferrian ilmenites in composition, temperature of formation, cooling history, transition-induced cation-ordered domain microstructure, and magnetic characteristics lends support to the placement of the transition curve in Figure 11. The simlarity also supports the hypothesis put forth by Lawson et al. (1981) that the "x" phase is the twin boundary and is the second magnetic phase necessary for the self-reversing mechanism. Therefore, self-reversal will be confined only to those ferrian ilmenites that crystallize in the $R\bar{3}c$ field and cool fast enough to supress coarsening of the twin domains in order to retain a high twin-boundary surface area.

The temperature of the transition and the kinetics of twin-domain growth and coarsening in natural ferrian ilmenites will depend on the composition and defect population. Solid solutions with Al_2O_3, Cr_2O_3, V_2O_3, $MgTiO_3$, and $MnTiO_3$ as well as deviations from cation-anion stoichiometry will raise or reduce the transition temperature, but more important will change the kinetics of domain growth or coarsening. The presence of increased defect population may increase Fe-Ti diffusion rates thus increasing twin-domain growth, but will also decrease coarsening rates by solute-drag on the domain boundaries. Therefore, impurities and defect densities will have competing roles on natural ferrian ilmenites.

There are a number of potential uses for the twin-domain microstructure that arises from the order-disorder transition. The presence of the twin domains indicates that the ilmenite passed through the transition, and therefore a minimum temperature of crystallization is known if T_c is known. The size and morphology of the twin domains will be a function of cooling rate, provided suitable corrections can be made for the effect of kinetics by impurities. The absence of twin domains in suitable compositions would indicate a maximum temperature of crystallization.

Conclusions

1. The transition between disordered $R\bar{3}c$ and ordered $R\bar{3}$ ilmenite-hematite has been redetermined. The transition was reversed for Ilm_{70} and lies between 1000 and 1050 °C.

2. Samples cooled through the transition contain a domain microstructure. The domains were shown by dark-field transmission electron microscopy to be twin-related by a 180° rotation about an axis parallel to **a**.

3. A structural model of the domain boundary suggests that the boundaries are disordered and thus antiferromagnetic and Fe enriched.

4. The size of the domains increases with increasing ilmenite component; this is directly related to the increase in T_c with increasing ilmenite component. The size of the domains also increases with increasing quench temperature above T_c.

5. The room-temperature saturation-magnetization intensity is directly related to the surface area per unit volume of the domain boundary and the long-range order of the cation-ordered domains. This is because the domains are ferrimagnetic with a strong magnetic moment whereas the boundary is parasitically ferromagnetic with a weak magnetic moment. The quenched products are mixtures of these two magnetic phases.

6. When the twin-boundary surface area exceeds the critical threshold of approximately 25×10^6 m^2/m^3, the

domain boundaries are able to couple antiferromagnetically with the cation-ordered domains, causing the sample to acquire a reverse thermoremanent magnetization during cooling from 600 °C in an applied field of 0.5 Oe. Therefore, the boundaries are the "x" phase of Ishikawa and Syono (1963).

7. It is only in quenched samples within the composition range Ilm_{51-73} that the boundary-surface area is able to exceed the critical threshold value. The dependence of critical twin-boundary surface area on the composition of the twins is unknown. Compositions more hematite-rich than Ilm_{50} (to the left of the tricritical point in Fig. 1) will not form ordered domains because of the miscibility gap; instead clustering will predominate rather than ordering. For compositions more ilmenite-rich than Ilm_{73}, the critical surface area may not be obtained because of the increased domain growth rate at the higher transition temperatures. Quenching Ilm_{80} into liquid N_2 from 1300 °C produces a domain microstructure an order of magnitude larger than the identical quench for Ilm_{70}. Somewhere between these two compositions, the domain-boundary surface area falls below the critical value of liquid N_2 quench rates. We also must keep in mind that the Curie temperature goes below room temperature for Ilm_{75-80}. This will complicate interpretation of the critical surface area. If we were able to measure TRM below room temperature, perhaps a different value of the critical surface area for reversal would hold.

Acknowledgments

We would especially like to acknowledge the contribution of Ginger Wandless to this study. She patiently and carefully prepared the friable synthetic samples for ion milling and TEM analysis. Many thanks to Princeton University and Robert Hargraves for access to the Rock Magnetics Laboratory and to Johns Hopkins University, David Veblen, and Ken Livi for the use of their TEM facilities. Howard Evans, Jr., USGS, kept us on the appropriate crystallographic path, and Bruce Moskowitz, University of California at Davis, kept us straight magnetically. Howard Evans, Jr., and Malcolm Ross, USGS, reviewed an early version of the manuscript.

References cited

Allen, S.M., and Cahn, J.W. (1976) Mechanism of phase transformations within the miscibility gap of Fe-rich Fe-Al alloys. Acta Metallurgica, 24, 425–437.

Amelinckx, S., and Van Landuyt, J. (1976) Contrast effects at planar interfaces. In H.-R. Wenk, Ed., Electron microscopy in mineralogy, p. 68–112. Springer-Verlag, Amsterdam.

Burton, B.P. (1982) Thermodynamic analysis of the systems $CaCO_3$-$MgCO_3$, α-Fe_2O_3, and Fe_2O_3-$FeTiO_3$. Ph.D. thesis, State University of New York, Stony Brook, New York.

Burton, B. (1984) Thermodynamic analysis of the system Fe_2O_3-$FeTiO_3$. Physics and Chemistry of Minerals, 11, 132–139.

Carmichael, C.M. (1961) The magnetic properties of ilmenite-hematite crystals. Proceedings of the Royal Society of London, A263, 508–530.

Carmichael, I.S.E. (1967) The iron-titanium oxides of salic volcanic rocks and their associated ferromagnesian silicates. Contributions to Mineralogy and Petrology, 14, 36–64.

Hirsch, P.B., Howie, A., Nicholson, R.B., Pashley, D.W., and Whelan, M.J. (1965) Electron microscopy of thin crystals, 549 p. Butterworths, London.

Hoffman, K.A. (1975a) Cation diffusion processes and self-reversal of thermoremanent magnetization in the ilmenite-hematite solid solution series. Geophysical Journal of the Royal Astronomical Society, 41, 65–80.

——— (1975b) On the kinetics of cation ordering in hemoilmenites and a reexamination of the self-reversal process. EOS, 56, 975.

Huebner, J.S. (1987) Use of gas mixtures at low pressure to specify oxygen and other fugacities of furnace atmospheres. In G.C. Ulmer and H.L. Barnes, Eds., Hydrothermal experimental techniques, p. 20–60. Wiley, New York.

Ishikawa, Y. (1958) An order-disorder transformation phenomena in the $FeTiO_3$-Fe_2O_3 solid solution series. Journal of the Physical Society of Japan, 13, 838–837.

——— (1962) Magnetic properties of ilmenite-hematite system at low temperature. Journal of the Physical Society of Japan, 17, 1835–1844.

Ishikawa, Y., and Akimoto, S. (1957) Magnetic properties of the $FeTiO_3$-Fe_2O_3 solid solution series. Journal of the Physical Society of Japan, 12, 1083–1098.

Ishikawa, Y., and Syono, Y. (1963) Order-disorder transformation and reverse thermoremanent magnetism in the $FeTiO_3$-Fe_2O_3 system. Journal of Physics and Chemistry of Solids, 24, 517–528.

Lawson, C.A. (1978) Problems in the use of evacuated, sealed silica tubes for synthesis of single-phase compositions in the system FeO-Fe_2O_3-TiO_2. Carnegie Institution of Washington Year Book 77, 917.

——— (1981) Magnetic and microstructural properties of minerals of the ilmenite-hematite solid solution series with special reference to the phenomenon of reverse thermoremanent magnetism, Ph.D. thesis, Princeton University, Princeton, New Jersey.

Lawson, C.A., and Nord, G.L., Jr. (1984) Remanent magnetization of a "paramagnetic" composition in the ilmenite-hematite series. Geophysical Research Letters, 11, 197–200.

Lawson, C.A., Nord, G.L., Jr., Dowty, E., and Hargraves, R.B. (1981) Antiphase domains and reverse thermoremanent magnetism in ilmenite-hematite minerals. Science, 213, 1372–1374.

Lawson, C.A., Nord, G.L., Jr., and Champion, D.E. (1987) Fe-Ti oxide mineralogy and the origin of normal and reverse remanent magnetization in dacitic pumice blocks from Mt. Shasta, California. Physics of Earth and Planetary Interiors, 46, 270–288.

Lerbekmo, J.F., Westgate, J.A., Smith, D.G.W., and Denton, G.H. (1975) New data on the character and history of the White River volcanic eruption, Alaska. In R.P. Suggate and M.M. Cresswell, Eds., Quaternary studies. Royal Society of New Zealand Bulletin, 13, 203–209.

Lindsley, D.H. (1965) Iron-titanium oxides. Carnegie Institution of Washington Year Book 64, 144–148.

——— (1976) The crystal chemistry and structure of oxide minerals as exemplified by the Fe-Ti oxides: Experimental studies of oxide minerals. Mineralogical Society of America, Reviews in Mineralogy, 3, L1–L88.

McLaren, A.C., and Phakey, P.P. (1969) Diffraction contrast from Dauphine twin boundaries in quartz. Physica Status Solidi, 31, 723–737.

Merrill, R.T., and Gromme, C.S. (1967) Non-reproducible self-reversal of magnetization in diorite. Journal of Geophysical Research, 74, 2014–2024.

Nagata, T., and Akimoto, S. (1956) Magnetic properties of ferromagnetic ilmenites. Geofisica Pura E Applicata, 34, 36–50.

Nord, G.L., Jr., and Lawson, C.A. (1988) The order-disorder transition in Fe_2O_3-$FeTiO_3$: Structure and migration kinetics of transformation-induced twin domain boundaries. In Phase transformations, 87, in press. Institute of Metals, London.

Raymond, K.N., and Wenk, H.R. (1971) Lunar ilmenite (refinement of the crystal structure). Contributions to Mineralogy and Petrology, 30, 135–140.

Smith, G.H., and Burge, R.E. (1962) The analytical representation of atomic scattering amplitudes for electrons. Acta Crystallographica, 15, 182–186.

Smith, C.S., and Guttman, L. (1953) Measurement of internal boundaries in three-dimensional structures by random sectioning. Transactions AIME, Journal of Metals, 197, 81–87.

Snow, J.D., and Heuer, A.H. (1973) Slip systems in Al_2O_3. Journal of the American Ceramic Society, 56, 153–157.

Uyeda, S. (1958) Thermo-remanent magnetization as a medium of paleo-

magnetism, with special reference to reverse thermo-remanent magnetism. Japanese Journal of Geophysics, 2, 1–123.

Wandless, M.-V., and Nord, G.L. Jr., (1986) Sample preparation techniques for transmission electron microscopy of geologic materials. U.S. Geological Survey Open-File Report 86-255, 20 p.

Westcott-Lewis, M.F., and Parry, L.G. (1971a) Magnetism in rhombohedral iron-titanium oxides. Australian Journal of Physics, 24, 719–734.

——— (1971b) Thermoremanence in synthetic rhombohedral iron-titanium oxides. Australian Journal of Physics, 24, 735–742.

Manuscript received July 25, 1988
Manuscript accepted September 30, 1988